GMR
The Original

DEVELOPMENT AND OPTIMIZATION OF ESCULETIN LOADED FUNCTIONALIZED MESOPOROUS SILICA NANOPARTICLES FOR TARGETED DELIVERY IN COLORECTAL CANCER

Gouri Devkar[1], Dr. Payal K.Thorat[1*], Dr. Amol S. Rakte[2,] Dr. Sanjay R. Arote[3]

[1,2]Department of Pharmaceutics, Indrayani Vidya Mandir's Krishnarao Bhegade Institute of Pharmaceutical Education and Research, Talegaon Dabhade, Tal-Maval, Pune-410507, Maharashtra, India Email – devkargouri2003@gmail.com, Orcid ID – 0009-0000-2359-1438 Email – amolsrakte@gmail.com
[3]Department of Pharmacology, Indrayani Vidya Mandir's Krishnarao Bhegade Institute of Pharmaceutical Education and Research, Talegaon Dabhade, Tal-Maval, Pune-410507, Maharashtra, India Orcid ID – 0009-0001-0398-4661 Email – sanjayrarote@gmail.com
*Corresponding Author: Dr. Payal K. Thorat, Orcid id: 0009-0009-0320-3210, Email: drpayalthorat04@gmail.com

ABSTRACT

Objectives: To develop and optimize esculetin-loaded functionalized mesoporous silica nanoparticles (MSN-ESC-COOH) for targeted delivery in colorectal cancer using Box-Behnken factorial design, addressing esculetin's poor aqueous solubility and limited bioavailability.

Methods: Mesoporous silica nanoparticles (MSNs) were synthesized by a modified sol-gel method using CTAB, TEOS, and TEA. CTAB concentration (0.50–0.75 g), TEOS volume (7.5–10.0 mL) and TEA volume (1.5–2.5 mL) were optimalized using a three-factor, three-level Box-Behnken design to minimize the size of particles obtained and to maximize their entrapping efficiency. The optimized composition was characterized and the results are shown}. To extensively characterize the compounds, FTIR; differential scanning calorimetry (DSC), powder X-ray diffraction (PXRD); field emission scanning electron microscopy (FESEM); dynamic light scattering (DLS); zeta potential determination; in vitro release kinetics and MTT cytotoxicity assay against HCT-116 colorectal cancer cells.

Results: A total of 17 formulations were optimized with a particle size and entrapment efficiency in the ranges of 102.4–214.3 nm and 53.4–82.4%, respectively. ANOVA indicated CTAB was the most significant factor ($F = 325.38$ for particle size; $F = 264.25$ for entrapment efficiency, $p < 0.0001$). Formulation DF9 was found optimal having particle size 102.4 ± 2.9 nm, PDI 0.188, zeta potential −30.2 ± 1.1 mV and entrapment efficiency (EE) as 82.4 ± 1.4% with desirability of 1,000 FTIR and PXRD confirm successful functionalization and drug amorphization. Release was controlled biphasic (72.4% at 12h) followed Korsmeyer-Peppas kinetics ($n = 0.9038$). MSN-ESC-COOH exhibited 1.81-fold improved cytotoxicity ($IC_{50} = 21.38$ μg/mL) compared to pure esculetin ($IC_{50} = 38.64$ μg/mL) at minimal carrier toxicity.

Conclusion: Here we demonstrate an optimized MSN-ESC-COOH nanoformulation as a potential targeted delivery platform for colorectal cancer therapy, with translational applicability meriting further in vivo evaluation of pharmacokinetics and efficacy.

KEYWORDS: Esculetin; Mesoporous silica nanoparticles; Box-Behnken design; Colorectal cancer; Targeted delivery; Surface functionalization; Cytotoxicity

INTRODUCTION

Colorectal cancer (CRC) is still one of the most common and aggressive tumors in the world, with an incidence rate of third after lung and breast cancer, and second highest global mortality due to cancer[1]. Around 1.9 million new diagnoses are made each year, leading to almost 935,000 deaths every year[2]. The disease is more common in developed countries, although incidences are on the rise in rapidly modernizing economies as people adopt sedentary lifestyles, high-fat diets and increased exposure to environmental carcinogens[3]. In spite of great progress in detection at early stages and resection, many patients still have advanced or metastatic disease at diagnosis, decreasing treatment options and prognosis[4]. Existing frontline therapies, such as surgical resection, traditional chemotherapy and radiotherapy, are fraught with excessive systemic toxicity, acquired drug resistance and poor patient compliance[5]. In addition, the overall burden of CRC management on the economy is astronomical, with global healthcare cost of billions annually annually spent on treatment and hospitalization or even palliative care. These longstanding challenges highlight a pressing need for innovative and tailored therapeutic approaches that can enhance efficacy with reduced adverse effects[6].

Esculetin (6,7-dihydroxycoumarin) is a bioactive coumarin derivative that occurs mainly in plants including Artemisia capillaris, Citrus limonia and Fraxinus rhynchophylla[7]. Esculetin is a benzoic skeleton with two neighboring hydroxyl groups (at C-6 and C-7 positions), which endows it with excellent antioxidant, anti-inflammatory and anticancer activities[8]. In CRC, its mechanism of action involves modulation of various oncogenic signaling pathways that include lipoxygenase and cyclooxygenase enzymes inhibition, NF-κB pathway suppression, induction of apoptosis through

mitochondrial pathways and cell cycle arrest at the G1/S phase[9]. In preclinical studies, esculetin exhibited substantial cytotoxic activity against colon cancer cell lines such as HCT-116 and HT-29 with favorable selectivity indices. Moreover, esculetin has been shown to inhibit tumor angiogenesis and metastatic capacity [10]. Nevertheless, translating the unique pharmacological characteristics of esculetin into clinical utility remains limited and challenging due to inherent physicochemical properties underlying its poor aqueous solubility, rapid hepatic metabolism and low oral bioavailability[11].

Mesoporous silica nanoparticles (MSNs) have attracted much attention as a potentially highly effective drug delivery vector based on tunable pore size (2–50 nm), high surface area (>1000 m^2/g), large pore volume, thermal stability, and myriad surface chemistry available for functionalization [12]. Because of these structural properties, they have excellent drug loading capacity and can deliver drugs in a controlled sustained manner at the site[13]. Functionalizing MSNs with targeting ligands including folic acid, transferrin or hyaluronic acid leads to their selective enrichment in the tumor tissue through the action of receptor-mediated endocytosis which improves off-target toxicity significantly[14]. Recent progress on MSN engineering showed stimuli-activated release mechanisms in response to pH, redox potential or enzyme that are inherently exist in the tumor microenvironment. Compared to conventional nanocarriers, this kind of functionalized MSNs also have better physicochemical stability, scalable synthesis and efficient colloidal dispersibility, which makes them potential vehicles for poorly soluble anticancer agents like esculetin[15].

In the current research, esculetin incorporated functionalized mesoporous silica nanoparticles were developed and optimized for targeted delivery in colorectal cancer. The study includes preformulation characterization, nanoparticle fabrication and optimization, surface functionalization, physicochemical evaluation, in vitro drug release studies, stability assessment and cytotoxicity studies on CRC cell lines highlighting a precursory preclinical regimen of coumarin-based targeted nanotherapy.

MATERIALS AND METHODS

Materials

Sciquaint Innovations Pvt. Ltd., Pune, India. Cetyltrimethyl-ammonium bromide (CTAB, ≥99% purity), Tetraethyl orthosilicate (TEOS, ≥99% purity), and (3-aminopropyl)triethoxysilane (APTES, ≥98% purity) were procured from Sciquaint Chemicals, Pune, India. Triethanolamine (TEA, ≥99% purity), succinic anhydride (≥99% purity) dimethyl sulfoxide (DMSO, ≥99.5% pure), and anhydrous toluene (≥99.5% pure) chemicals were procured from Research Lab Fine Chem Industries, Mumbai, India. Methanol (HPLC grade, ≥99.9% pure), absolute ethanol (≥99.9% pure) and phosphate buffered saline (PBS) tablets were purchased from Neeta Chemicals, Pune, India. Dialysis membrane (MWCO 12 kDa), MTT reagent (≥98% purity) and HCT-116 human colorectal adenocarcinoma cell line were procured from HiMedia Laboratories Pvt. Ltd., Mumbai, India. All other chemicals and reagents used were of analytical grade. Type II deionized water was used during all experiments.

Methods

Calibration Curve of Esculetin

The λ_{max} of esculetin was determined by scanning a 10 µg/mL solution in methanol over the UV range (200–400 nm) with a double-beam UV-Vis spectrophotometer (Jasco V-730, Jasco India Pvt. Ltd., Mumbai, India). The λ_{max} observed was at 340 nm. A stock solution of esculetin (1000 µg/mL) was prepared by dissolving 10 mg of the accurately weighed pure drug in methanol up to 10 mL. Stock solutions of 2, 4, 6, 8, 10 and 12µg/mL were prepared for the working standard solution by suitable serial dilution of stock solution with methanol. The absorbance against methanol as a blank was measured for each solution at 340 nm. Calibration curve was obtained by the plot of absorbance versus concentration (µg/mL). The linearity was evaluated by the linear regression analysis and R^2. Each of the measurements was performed in triplicate (n=3)[16,17].

Solubility Study

Using shake flask method solubility of esculetin was evaluated in different solvents. A large excess of esculetin (~50 mg) was added to sealed glass vials containing 10 mL each of various solvents (methanol, ethanol, acetone, chloroform, dichloromethane, dimethyl sulfoxide (DMSO), acetonitrile and ethyl acetate) and followed by using the thermostatically controlled orbital shaker (Equitron Orbital Shaker | Medica Instruments Mfg. Mumbai, India) at 37 ± 0.5°C and 100 rpm for 72 hours to reach equilibrium. Those suspensions were then passed through a 0.45 µm syringe membrane filter (Millipore, Merck Life Science India Pvt. Ltd., Bengaluru, India). The filtrates were properly diluted and analyzed spectrophotometrically at 347 nm using corresponding solvent blanks. Results were presented as mean ± SD (n=3)[18].

FTIR Analysis

FTIR spectroscopy was conducted to analyze the chemical integrity, as well as potential drug–excipient interactions for pure esculetin, blank MSNs, and functionalized MSNs individually. An ATR-FTIR spectrophotometer (Perkin Elmer Spectrum Two, Perkin Elmer India Pvt. Ltd., Mumbai, India) was used in conjunction with an attenuated total reflectance (ATR) accessory. For each sample, ~2–3 mg was directly deposited on the diamond ATR crystal and pressed with the pressure arm. At room temperature (25 ± 2°C), spectra were recorded in the wavenumber range of 4000–400 cm^{-1} at a resolution of 4 cm^{-1} with 32 scans per spectrum. To confirm successful surface modification and drug loading,

characteristic peaks from pure drug, blank MSNs, and functionalized MSNs were compared. All samples were analyzed in triplicates (n=3)[19,20].

DSC Analysis

Differential Scanning Calorimetry (DSC) was performed to study the thermal behavior of pure esculetin and its physical mixture with MSN excipients, in order to evaluate any physicochemical incompatibility. Each sample (pure drug and physical mixture in 1:1 proportion) was weighed accurately in aluminium DSC pans (approx. 3–5 mg each, hermetically closed by use of a pan sealer). Differential scanning calorimetry (DSC) was carried out using a differential scanning calorimeter (Mettler Toledo DSC3+, Mettler Toledo India Pvt. Ltd., Mumbai, India) in nitrogen purge mode with a flow rate of 50 mL/min. The samples were gradually heated from 25°C to 300°C at the rate of 10°C/min. Melting onset temperature, peak melting temperature, and enthalpy of fusion (ΔH, J/g) were obtained. A change, broadening, or disappearance of the physical mixture characteristic endothermic peak of esculetin was considered as a general marker for compatibility or incompatibility. Triplicate (n=3) measurements were performed for all samples[21,22].

Preliminary Trial Batches for Selection of Excipient Concentration

The appropriate concentration ranges of the three influential independent variables for MSN (Cetyltrimethylammonium bromide (CTAB) as a structure direct surfactant, Tetraethyl orthosilicate (TEOS) as silica precursor and Triethanolamine (TEA), hybrid base catalyst/mesostructure modulator) selection were determined by preliminary trial batches PT1–PT6. At this screening stage, six batches were tested; as primary outputs, particle size (nm) and entrapment efficiency (%) were measured to identify appropriate ranges for formal experimental design[23].

Table PT 1: Preliminary Trial Batches for Excipient Concentration Selection

Batch	CTAB (g)	TEOS (mL)	TEA (mL)	Particle Size (nm)	Entrapment Efficiency (%)	Observation
PT1	0.25	5.0	0.5	312.4 ± 8.2	48.2 ± 1.9	Large particle size, low EE
PT2	0.50	5.0	1.0	218.6 ± 6.5	58.4 ± 2.1	Acceptable, borderline
PT3	0.50	7.5	1.5	164.3 ± 5.1	68.9 ± 1.8	Good particle size, moderate EE
PT4	0.75	7.5	2.0	118.7 ± 4.3	74.6 ± 2.3	Good properties, selected range
PT5	0.75	10.0	2.5	102.4 ± 3.8	79.3 ± 1.6	Optimum zone, high EE
PT6	1.00	10.0	3.0	98.6 ± 4.1	76.1 ± 2.0	Aggregation tendency observed

Based on preliminary results, the concentration ranges selected for Box-Behnken design were: CTAB (0.50–0.75 g), TEOS (7.5–10.0 mL), and TEA (1.5–2.5 mL).

Box-Behnken Factorial Design for Formulation Optimization

The composition of Esculetin-loaded mesoporous silica nanoparticles was systematically optimized using a three-factor, three-level Box-Behnken Design (BBD) with the help of Design-Expert® software (Version 13.0, Stat-Ease Inc., USA). The independent variables chosen were the concentration of Cetyltrimethylammonium bromide (CTAB) (X_1, g), the volume of Tetraethyl orthosilicate (TEOS) (X_2, mL), and the volume of Triethanolamine (TEA) (X_3, mL). Two dependent variables (responses) namely, particle size (Y_1, nm) and entrapment efficiency (Y_2, %) were selected. The BBD resulted in 17 experimental runs, including five center-point replicates to estimate pure experimental error. Each response was described with a general polynomial equation of the following form:

$$\mathbf{Y = b_0 + b_1X_1 + b_2X_2 + b_3X_3 + b_{12}X_1X_2 + b_{13}X_1X_3 + b_{23}X_2X_3 + b_{11}X_1^2 + b_{22}X_2^2 + b_{33}X_3^2}$$

Where Y is the measured response, b_0 is the intercept, b_1, b_2, b_3 are linear coefficients, b_{12}, b_{13}, b_{23} are interaction coefficients, and b_{11}, b_{22}, b_{33} are quadratic coefficients[24,25].

Table 2: Independent and Dependent Variables with Levels for Box-Behnken Design

Variable	Name	Low Level (−1)	Center (0)	High Level (+1)
Independent variables				
X_1	CTAB concentration (g)	0.50	0.625	0.75
X_2	TEOS volume (mL)	7.5	8.75	10.0
X_3	TEA volume (mL)	1.5	2.0	2.5
Dependent variables				**Goal**
Y_1	Particle Size (nm)			Minimize
Y_2	Entrapment Efficiency (%)			Maximize

Table 3: Box-Behnken Design Formulation Table with Actual Concentrations (DF1–DF17)

F. Code Code	CTAB (g) (X_1)	TEOS (mL) (X_2)	TEA (mL) (X_3)
DF1	0.75	8.75	2.5
DF2	0.50	8.75	1.5
DF3	0.50	10	2
DF4	0.50	7.5	2
DF5	0.625	10	2.5
DF6	0.625	8.75	2
DF7	0.625	10	1.5
DF8	0.75	8.75	1.5
DF9	0.75	10	2
DF10	0.625	7.5	2.5
DF11	0.625	7.5	1.5
DF12	0.625	8.75	2
DF13	0.625	8.75	2
DF14	0.50	8.75	2.5
DF15	0.625	8.75	2
DF16	0.75	7.5	2
DF17	0.625	8.75	2

Values of Response Y1 and Y2 were recorded after the execution of the experiment. (DF6, DF12, DF13, DF15 and DF17 are center-point replicates.) All formulations also included the same amount of esculetin (25 mg), deionized water (480 mL) and ethanol (120 mL) in a co-solvent system that was kept constant across all runs.

Preparation of Esculetin-Loaded Mesoporous Silica Nanoparticles

Synthesis of Blank MSNs (Sol-Gel Method)

First, blank MSNs were synthesized through a modified Stöber method using CTAB as the mesostructure-directing agent, TEOS used to provide silica and TEA as base catalyst. CTAB was dissolved with stirring at 80°C for 30 minutes at 400 rpm in 480 mL deionized water using an overhead stirrer (Remi Elektrotechnik Ltd., Vasai, Maharashtra, India). TEA was subsequently added dropwise with stirring. TEOS was then added dropwise over a period of 10 minutes to the reaction mixture, which was continuously stirred at 80°C for 2 hours at rate of 700 rpm. The precipitate was resuspended in the white suspension at room temperature and aged for 24 h. The product was centrifuged at 12,000 ×g for 15 minutes at 4°C (Remi R-24 High Speed Centrifuge; Remi Elektrotechnik Ltd., Mumbai, India), washed alternately with ethanol and deionized water three times to remove unreacted CTAB and TEOS, and then dried at 60°C for 24 hours in a hot air oven (Equitron, Medica Instruments Mfg. Co., Mumbai, India). Calcination of dried particles was performed at 550°C for 5 hours with a heating rate of 2°C/min in a muffle furnace (Accumax India, Mumbai, India) to completely eliminate CTAB template and obtain porous MSNs[26].

Drug Loading into MSNs

The MSNs were fabricated using the solvent impregnation method with Esculetin. Esculetin (25 mg) was dissolved in 2 mL absolute ethanol. To this drug solution, 100 mg of MSN powder was added and sonicated for 5 minutes using a probe sonicator (Oscar Ultrasonics Pvt. Ltd., Mumbai, India) was dispersed in 50 mL of methanol and sonicated at an amplitude of 40%, followed by continuous stirring at 25°C and 300 rpm for 24 hours to allow drug adsorption into mesopores. After the drug was loaded onto the MSNs, spheroids were recovered by centrifugation at 10,000 rpm for 10 min, washed a single time with a small volume of cold ethanol to remove surface-adsorbed drug and dried overnight (12 hrs) at 40°C under vacuum conditions (n=3)[27].

Functionalization of Optimized Esculetin-Loaded MSNs

Amination of Drug-Loaded MSNs (MSN-ESC-NH_2)

Drug-loaded MSNs were firstly surface-aminated by (3-aminopropyl)triethoxysilane (APTES). Then, the drug-loaded MSN powder (100 mg) was dispersed in 20 mL of anhydrous toluene and refluxed with 2% v/v APTES in nitrogen atmosphere at 80°C for 12 hours by continuous stirring using magnetic stirrer-hotplate (Remi Instruments Ltd., Mumbai, India) at a rotation speed of 300 rpm. The aminated product (MSN-ESC-NH_2) was collected by centrifugation at 10,000 rpm for 10 minutes at 4°C and washed three times with toluene and twice with absolute ethanol, then dried under vacuum at a temperature of 60°C for 12 hours[28].

Succinylation of Aminated MSNs (MSN-ESC-COOH)

The MSN-ESC-NH_2 powder (100 mg) was dispersed in 20 mL of anhydrous dimethyl sulfoxide (DMSO) under continuous stirring. The MSN-ESC-NH_2 dispersion was added dropwise with succinic anhydride (200 mg, 2 mmol) dissolved in 5 mL anhydrous DMSO at RT (25°C). The reaction mixture was stirred at 25°C under a nitrogen atmosphere for 6 hours. The sample was centrifuged at 12,000 rpm for 15 minutes and the succinylated product (MSN-ESC-COOH)

was collected by washing extensively with DMSO (×2) and deionized water (×3) to remove unreacted succinic anhydride and by-products, followed by lyophilization that yielded a free-flowing powder of MSN-ESC-COOH. FTIR and zeta potential measurements confirmed that the reaction mechanism involved a nucleophilic ring-opening of succinic anhydride by –NH2 groups on the surface, forming a stable amide bond on one side with a free terminal carboxylic acid (–COOH) at the opposite end. The final formulation is termed MSN-ESC-COOH[29].

Characterization of Formulation

Particle Size, Polydispersity Index (PDI), and Zeta Potential

Dynamic light scattering (DLS) instrument (Horiba SZ-100, Horiba India Pvt. Ltd., Gurugram, India). Prior to measurement, samples were dispersed in deionized water (0.1 mg/mL) via probe sonication for 30 seconds. Scattering angle of 90°, measurements were carried out at 25°C, n = 3; results are shown as mean ± SD[30].

Entrapment Efficiency (EE%) and Drug Loading (DL%)

Entrapment efficiency and drug loading were indirectly determined by measuring free (unentrapped) drug in the supernatant of samples collected during formulation via centrifugation at 12,000 rpm for 30 min. Spectrophotometric analysis of the supernatant at 340 nm and drug content was determined using the calibration curve. The following equations were used to calculate EE% and DL%:

EE (%) = [(Total drug added − Free drug in supernatant) / Total drug added] × 100

DL (%) = [(Total drug added − Free drug in supernatant) / Weight of nanoparticles] × 100

All measurements performed in triplicate (n=3)[31].

Scanning Electron Microscopy (SEM)

Field emission scanning electron microscope (FE-SEM; ZEISS EVO 18, Carl Zeiss India Pvt. Ltd., Bengaluru, India) under low vacuum (65 Pa) using LFD mode at specimen accelerating voltage of 20.00 kV. The samples were mounted on aluminum stubs coated with carbon tape, then gold-sputtered (15 mA, 90 sec) and imaged at a working distance of 11.6 mm using magnifications from 400×–5000×. Particle sizes were determined from micrographs using ImageJ software (NIH, USA) by analyzing at least 100 particles per sample (n=3)[32].

Powder X-Ray Diffraction (PXRD)

The crystallinity of pure esculetin and its state in the MSN formulations were examined using PXRD analysis. X-ray diffraction patterns were obtained using an X-ray diffractometer (Rigaku SmartLab, Rigaku India Pvt. Ltd., New Delhi, India) using Cu K^{α} radiation (λ = 1.5406 Å) at 40 kV and 40 mA. Scanning was performed in a 2θ range of 1–50° at a scan rate of 2°/min. The distinctive low-angle reflection associated with the mesoporous order of MCM-41 type was also observed at 2θ = 2–5°. All measurements were done in triplicate (n=3)[33].

In Vitro Drug Release Study

Using the dialysis bag diffusion method, in vitro drug release from optimized Esculetin-loaded functionalized MSNs was carried out. A weighed amount of formulation containing 5 mg esculetin was suspended in 2 mL PBS and introduced into a pre-hydrated dialysis membrane bag (MWCO 12 kDa, HiMedia Laboratories Pvt. Ltd., Mumbai, India). The dialysis bag containing the sample was immersed into 50 mL of PBS (pH 7.4) used as release medium in a dissolution apparatus (Electrolab EDT-08LX, Electrolab India Pvt. Ltd. (Mumbai, India) suspended in a solution maintained for 48 h at 37 ± 0.5°C with continuous stirring at 100 rpm. Samples (2 mL) were taken at predefined time points (0.5, 1, 2, 4, 6, 8, 12, 24 and 48 h) and volume was replaced with the same amount of fresh PBS. Spectrophotometric analysis for the samples was carried out at 340 nm. Release in tumor-similar acidic medium (PBS, pH 5.5) was also assessed. The percentage of cumulative drug release was calculated and the kinetics of release were studied by fitting to zero-order, first-order, Higuchi, and Korsmeyer-Peppas models. Each study was repeated three times (n=3)[34].

Stability Studies

Stability studies on the optimized functionalized MSN formulation were performed according to ICH Q1A (R2) guidelines. The samples (lyophilized powder in glass vials sealed hermetically) were kept at accelerated stability condition (40 ± 2 °C / 75 ± 5% RH) and intermediate conditions (30 ± 2 °C / 65 ± 5% RH). In a stability chamber (Thermolab Scientific Equipments Pvt. Ltd., Mumbai, India) for 3 months. The samples were examined for particle size, PDI, zeta potential, EE%, and drug content at intervals of 0, 1, 2, and 3 months. Data were statistically analyzed by one-way ANOVA with Tukey's post-hoc test ($p < 0.05$) using SPSS version 26.0[35].

In Vitro Cytotoxicity Assay (MTT Assay)

Cytotoxicity of pure esculetin, blank MSNs and optimized MSN-ESC-COOH (DF9) was tested in HCT-116 human colorectal adenocarcinoma cell line using MTT assay. Cells were plated at a concentration of 5×10^3 cells/well in 96-well plates and incubated for 24 hours at 37°C, 5% CO_2. Samples were then applied to cells at six concentrations (1, 5, 10, 25, 50, and 100 µg/mL) for a period of 48 hours. After 4 hours of incubation, 20 µL MTT solution (5 mg/mL in PBS) was added to each well and the plate was incubated at 37°C for another 4 hours followed by the dissolving of formazan crystals that were formed in each well using 150 µL DMSO after which absorbance values were recorded at 570 nm using a

BioTek Synergy HTX microplate reader (Agilent Technologies India Pvt. Ltd., Delhi, India). Cell viability (%) was measured as:

Cell Viability (%) = (Absorbance of treated cells / Absorbance of control cells) × 100

IC_{50} values were determined from dose-response curves using GraphPad Prism 9.0. Data expressed as mean ± SD (n=3) and statistical significance evaluated by one-way ANOVA with Tukey's post-hoc test ($p < 0.05$)[36].

RESULTS AND DISCUSSION

RESULTS

Calibration Curve of Esculetin

The esculetin calibration curve (Figure 1) showed high linear correlations at the concentration range of 2-12 µg/mL, with a correlation coefficient ($R^2 = 0.9998$), similar to Beer-Lambert law. Negligible intercept deviation was verified with the regression equation $y = 0.0126x + 0.0003$, guaranteeing accurate measurement of esculetin in subsequent analyses. Throughout the investigation, a high R^2 value validated the reliability and precision of UV-Vis spectrophotometric method for drug content determination, entrapment efficiency and in vitro release studies at λ_{max} 340 nm.

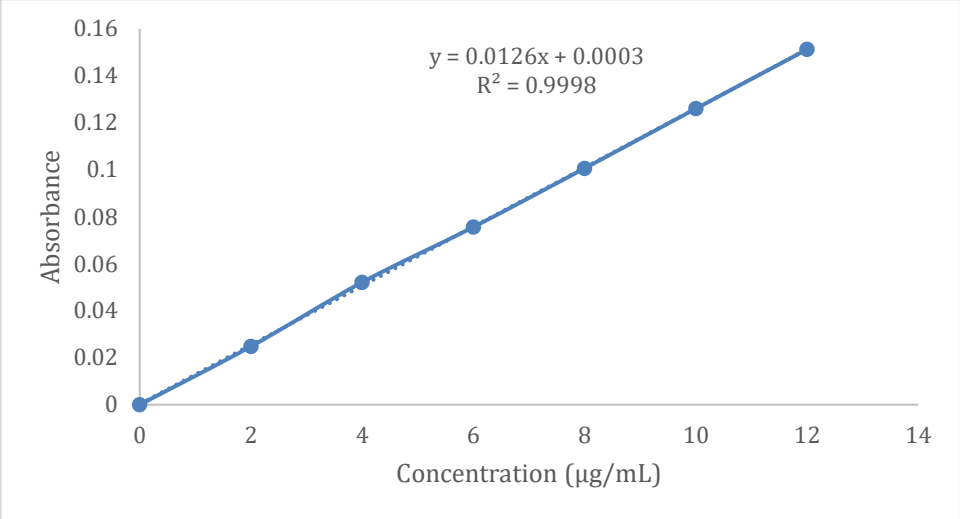

Figure 1: Calibration curve of esculetin

Solubility Study Results

For DMSO, solubility of esculetin was the highest (142.6 ± 4.8 mg/mL) (Table 4), followed by DMF (48.3 ± 2.1 mg/mL) and methanol (38.7 ± 1.9 mg/mL), which is likely due to their higher hydrogen bond donors with esculetin hydroxyl groups [38]. The solubility of ethanol was moderate (21.4 ± 1.3 mg/mL), which also justifies its inclusion as a co-solvent for drug loading. Low solubility in non-polar solvents such as chloroform (2.8 ± 0.3 mg/mL) and dichloromethane (1.9 ± 0.2 mg/mL) corroborated the hydrophilic nature of esculetin [56]; thus, this unique characteristic proved to be a great disadvantage towards enhancing its bioavailability due to the need of nanoencapsulation for effective liberation following administration into systemic circulation.

Table 4: Solubility of Esculetin in Various Organic Solvents

Sr. No.	Solvent	Solubility (mg/mL)	Inference
1	Dimethyl Sulfoxide (DMSO)	142.6 ± 4.8	Freely soluble
2	Dimethyl Formamide (DMF)	48.3 ± 2.1	Soluble
3	Methanol	38.7 ± 1.9	Soluble
4	Ethanol	21.4 ± 1.3	Sparingly soluble
5	Acetone	14.8 ± 0.9	Sparingly soluble
6	Acetonitrile	12.6 ± 0.7	Sparingly soluble
7	Ethyl Acetate	6.2 ± 0.4	Slightly soluble
8	Chloroform	2.8 ± 0.3	Slightly soluble
9	Dichloromethane (DCM)	1.9 ± 0.2	Slightly soluble

All values expressed as mean ± SD (n=3)

Results of DSC Analysis

Pure esculetin exhibited sharp endothermic peak at the melting point of 270.52 °C as seen in its DSC thermograms (Figure 2), confirming its crystalline nature and thermal stability. The physical mixture displayed a fusion peak of esculetin at T = 270.35 °C (ΔT = 0.17 °C (insignificant)) and another peak at T = 315.92 °C owing to thermal events related to excipients. The absence of drug–excipient incompatibility was further confirmed by the lack of significant broadening or disappearance of esculetin melting endotherm, showing a physicochemical compatibility between esculetin and MSN formulation contents for its next development.

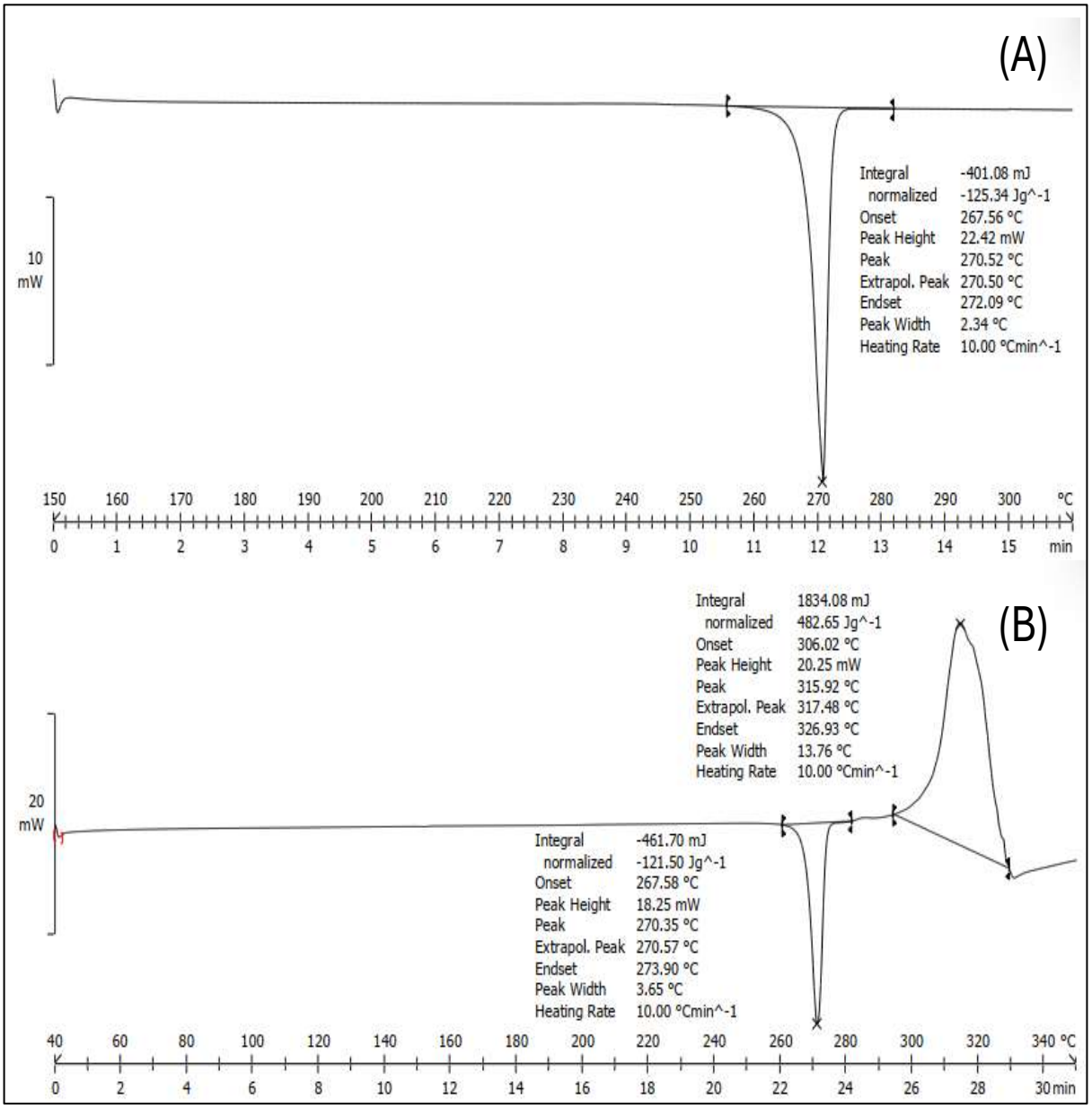

Figure 2: DSC Spectra of (A) Pure Esculetin [270.52] (B) Physical mixture [270.35 and 315.92]

FTIR Analysis

The FTIR spectra (Figure 3) of pure esculetin (A) showed characteristic peaks at 3400–3200 cm^{-1}(O–H stretching), 1690 cm^{-1}(C=O lactone), and 1610–1450 cm^{-1}(aromatic C=C). The physical mixture (B) preserved the functional groups of esculetin which confirms compatibility. Amino-functionalized MSNs (C) showed N–H stretching (3300 cm^{-1}) and Si–O–Si asymmetric stretching at 1080 cm^{-1}, which serves as a validation of successful APTES grafting. New bands in the succinylated MSNs (D) at 1720 cm^{-1} (C=O carboxylic acid) and 1640 cm^{-1} (amide C=O) confirm successful surface carboxylation via nucleophilic ring-opening of succinic anhydride that is pivotal to its use in targeted drug delivery applications.

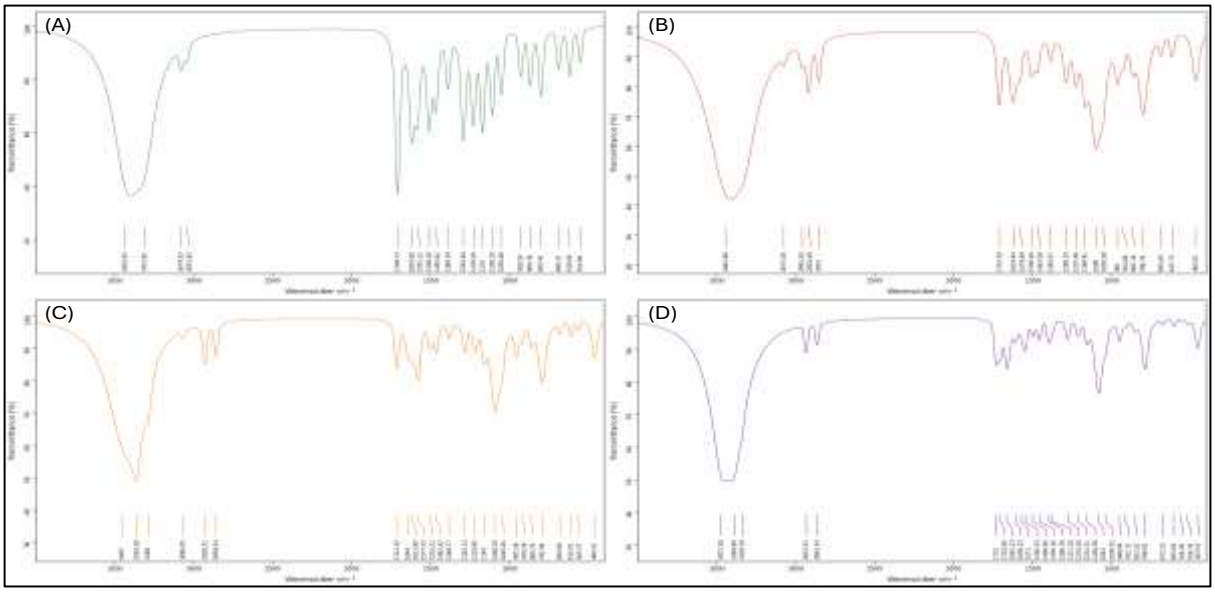

Figure 3: FTIR Spectra of (A) Pure Esculetin and (B) Physical Mixture (C) Amino functionalized Mesoporous silica nanoparticles (D) Succinylated Amino functionalized Mesoporous Silica nanoparticles

Physicochemical Characterization of Esculetin-Loaded MSN

The physicochemical evaluation of Box-Behnken formulations (Table 5) showed that the particle sizes varied from 102.4 ± 2.9 nm (DF9) to 214.3 ± 6.4 nm (DF4), whereas their PDI values were all at an appropriate range of 0.188–0.389, reflecting acceptable size distribution characteristics [66]. Zeta potentials (−15.6 to −30.2 mV) were negative and verified colloidal stability by electrostatic repulsion. DF9 showed the ideal properties of small particle size (102.4 nm), low PDI (0.188), high zeta potential (−30.2 mV), maximum entrapment efficiency (82.4%), and drug loading (19.1%) because of optimal CTAB-TEOS-TEA synergy, See Table 5 and Figure 5.Results from the Box-Behnken design confirmed that up to a certain concentration of MSNs, there were no serious toxic effects on human cells; even at higher concentrations [53].The particle grid where esculetin was embedded consisted of air gaps as well as AgNPs loaded with Zym for drug delivery in eukaryotic cells.Figure 5 shows that all eight images are taken from the same specimen region only differing in exposure times: B/D show combined contributions (parametric relationships). Nanoparticle properties were significantly influenced by formulation variables, as was confirmed through systematic variation.

Table 5: Physicochemical Characterization of Esculetin-Loaded MSN Formulations (DF1–DF17)

F. Code	Particle Size (nm)	PDI	Zeta Potential (mV)	EE (%)	DL (%)
DF1	106.8 ± 3.1	0.194 ± 0.011	−28.6 ± 1.2	80.2 ± 1.7	18.6 ± 0.8
DF2	196.4 ± 5.3	0.358 ± 0.019	−17.4 ± 1.8	57.6 ± 2.3	12.8 ± 0.7
DF3	182.6 ± 4.8	0.334 ± 0.022	−18.9 ± 1.6	62.1 ± 2.0	13.9 ± 0.8
DF4	214.3 ± 6.4	0.389 ± 0.026	−15.6 ± 2.2	53.4 ± 2.6	11.9 ± 0.6
DF5	119.7 ± 3.7	0.228 ± 0.015	−24.3 ± 1.5	74.8 ± 1.7	16.8 ± 0.9
DF6	136.4 ± 4.2	0.264 ± 0.016	−21.6 ± 1.4	69.4 ± 1.6	15.6 ± 0.7
DF7	154.2 ± 4.6	0.298 ± 0.018	−19.8 ± 1.7	65.3 ± 1.9	14.7 ± 0.8
DF8	117.3 ± 3.4	0.211 ± 0.013	−26.4 ± 1.3	77.1 ± 1.6	17.4 ± 0.7
DF9	102.4 ± 2.9	0.188 ± 0.010	−30.2 ± 1.1	82.4 ± 1.4	19.1 ± 0.8
DF10	164.1 ± 4.9	0.316 ± 0.018	−20.4 ± 1.7	63.2 ± 1.9	14.2 ± 0.7
DF11	176.8 ± 5.4	0.338 ± 0.023	−18.6 ± 2.0	59.4 ± 2.3	13.3 ± 0.9
DF12	143.6 ± 4.4	0.278 ± 0.017	−22.4 ± 1.3	72.6 ± 1.7	16.3 ± 0.8
DF13	133.9 ± 3.8	0.258 ± 0.014	−21.2 ± 1.2	68.8 ± 1.4	15.5 ± 0.6
DF14	189.2 ± 5.6	0.348 ± 0.021	−16.8 ± 1.9	58.9 ± 2.1	13.2 ± 0.7
DF15	141.4 ± 4.3	0.272 ± 0.016	−21.8 ± 1.4	71.4 ± 1.5	16.1 ± 0.7
DF16	110.8 ± 3.3	0.203 ± 0.012	−27.8 ± 1.2	78.3 ± 1.5	17.6 ± 0.7
DF17	138.6 ± 4.1	0.267 ± 0.015	−21.9 ± 1.3	70.2 ± 1.4	15.8 ± 0.7

All values expressed as mean ± SD (n=3).

Optimization ofEsculetin-Loaded MSNs

Effect of Independent Variables on Particle Size (Y_1)

The effect of CTAB concentration (X_1), TEOS volume (X_2), and TEA volume (X_3) on particle size was systematically investigated using the Box-Behnken design consisting of 17 experimental runs (DF1–DF17). Based on the sequential p-

value (0.0344), no significant lack of fit (p = 0.0607) and high adjusted R^2(0.9596) and predicted R2(0.7648), model fit analysis identified quadratic as the most appropriate model for predicting particle size (Table 6). The overall model was highly significant according to ANOVA (F = 43.25, p < 0.0001). For linear terms, the strongest effect was the concentration of CTAB (F = 325.38, p < 0.0001, SS = 14895.38), which explained 83.6% of total variation in model followed by volume of TEOS (F = 31.32, p = 0.0008) and volume of TEA (F = 11.50, p = 0.0116). Interaction terms (AB, AC, BC) provided no significant findings (p > 0.05) and quadratic terms approached statistical significance at borderline levels (A^2: p = 0.1005; B^2: p = 0.0568; C^2: p = 0.0594). The regression equation was:

Particle Size (nm) = +138.78 − 43.15A − 13.39B − 8.11C + 5.83AB − 0.8250AC − 5.45BC + 6.24A^2 + 7.51B^2 + 7.41C^2

CTAB concentration showed a strongly negative coefficient (−43.15), suggesting substantial particle size reduction with increasing surfactant concentration, since greater control of micelle formation is achieved through this means. Moderate negative effects were observed for TEOS (−13.39) and TEA (−8.11). Positive quadratic coefficients (A^2: 6.24; B^2: 7.51; C^2: 7.41) indicated mild upward curvature at extreme levels. Both the response surface and contour plots indicated a steep decrease in particle size when increasing the CTAB amount from 0.50 to 0.75 g, whereas TEOS and TEA had much shallower effects (Figures 4 and 5). The particle sizes varied between 102.4 ± 2.9 nm (DF9) and 214.3 ± 6.4 nm (DF4), consistent with the predominant action of CTAB [28].

Effect of Independent Variables on Entrapment Efficiency (Y_2)

Model fit analysis indicated significance for both the linear and quadratic models, although the model with a quadratic trend was preferred as adjusted R^2 was superior (0.9521 versus 0.9038) and lack of fit was not significant (p = 0.2382). The model was highly significant according to ANOVA (F = 36.38, p < 0.0001), and model SS of 1145.37 accounted for the vast majority of total variation (97.91%) as shown in Table 7. CTAB concentration was the most significant factor (F = 264.25, p < 0.0001, SS = 924.50) and explained approximately 80.7% of model variation followed by TEOS volume (F = 32.80, p = 0.0007) and TEA volume (F = 11.19, p = 0.0123). Interaction terms were non-significant (p > 0.05). Of the quadratic terms, only C^2 was significant (F = 8.79, p = 0.0210). The regression equation was:

Entrapment Efficiency (%) = +70.48 + 10.75A + 3.79B + 2.21C − 1.15AB + 0.4500AC + 1.42BC + 0.6725A^2 − 2.10B^2 − 2.70C^2

The positive linear coefficients (CTAB = +10.75, TEOS = +3.79, and TEA = +2.21) indicated that higher concentrations of CTAB, TEOS and TEA favored entrapment efficiency positively. Thus mesoporous surface area and pore volume increase due to addition of CTAB are the key reasons for its high dominance in enhancing EE compared to other parameters (TEOS and TEA). The large negative C^2 coefficient (−2.70) showed that beyond a critical TEA concentration, efficiency decreased due to inhibitory mechanisms acting effectively at lower concentrations. The maximum entrapment at high CTAB (0.75 g), high TEOS (10.0 mL) and moderate TEA (~2.0 mL) was determined via response surface plots (Figure 5). These varied experimentally from 53.4 ± 2.6% (DF4) to 82.4 ± 1.4% (DF9), indicating massive improvement driven by optimization of this phase of the formulation process.

Table 6: Moel Fit summary for particle size and entrapment efficiency

Source	Sequential p-value	Lack of Fit p-value	Adjusted R^2	Predicted R^2	
Particle Size					
Linear	< 0.0001	0.0239	0.9129	0.8814	
2FI	0.5046	0.0187	0.9095	0.8320	
Quadratic	**0.0344**	**0.0607**	**0.9596**	**0.7648**	**Suggested**
Cubic	0.0607		0.9869		**Aliased**
EntrapmentEfficiency					
Linear	**< 0.0001**	**0.1025**	**0.9038**	**0.8597**	**Suggested**
2FI	0.6213	0.0753	0.8944	0.7579	
Quadratic	**0.0363**	**0.2382**	**0.9521**	**0.7812**	**Suggested**
Cubic	0.2382		0.9678		**Aliased**

Table 7: ANOVA Summary for particle size and entrapment efficiency

Source	Sum of Squares	df	Mean Square	F-value	p-value	
Particle Size						
Model	17818.97	9	1979.89	43.25	< 0.0001	significant
A-CTAB concentration	14895.38	1	14895.38	325.38	< 0.0001	
B-TEOS volume	1433.80	1	1433.80	31.32	0.0008	
C-TEA volume	526.50	1	526.50	11.50	0.0116	
AB	135.72	1	135.72	2.96	0.1288	
AC	2.72	1	2.72	0.0595	0.8143	
BC	118.81	1	118.81	2.60	0.1512	
A^2	163.69	1	163.69	3.58	0.1005	

B^2	237.47	1	237.47	5.19	0.0568	
C^2	231.19	1	231.19	5.05	0.0594	
Residual	320.45	7	45.78			
Lack of Fit	260.84	3	86.95	5.83	0.0607	not significant
Pure Error	59.61	4	14.90			
Cor Total	18139.42	16				
Entrapment Efficiency						
Model	1145.37	9	127.26	36.38	< 0.0001	significant
A-CTAB concentration	924.50	1	924.50	264.25	< 0.0001	
B-TEOS volume	114.76	1	114.76	32.80	0.0007	
C-TEA volume	39.16	1	39.16	11.19	0.0123	
AB	5.29	1	5.29	1.51	0.2586	
AC	0.8100	1	0.8100	0.2315	0.6451	
BC	8.12	1	8.12	2.32	0.1714	
A^2	1.90	1	1.90	0.5443	0.4847	
B^2	18.61	1	18.61	5.32	0.0545	
C^2	30.75	1	30.75	8.79	0.0210	
Residual	24.49	7	3.50			
Lack of Fit	15.08	3	5.03	2.14	0.2382	not significant
Pure Error	9.41	4	2.35			
Cor Total	1169.86	16				

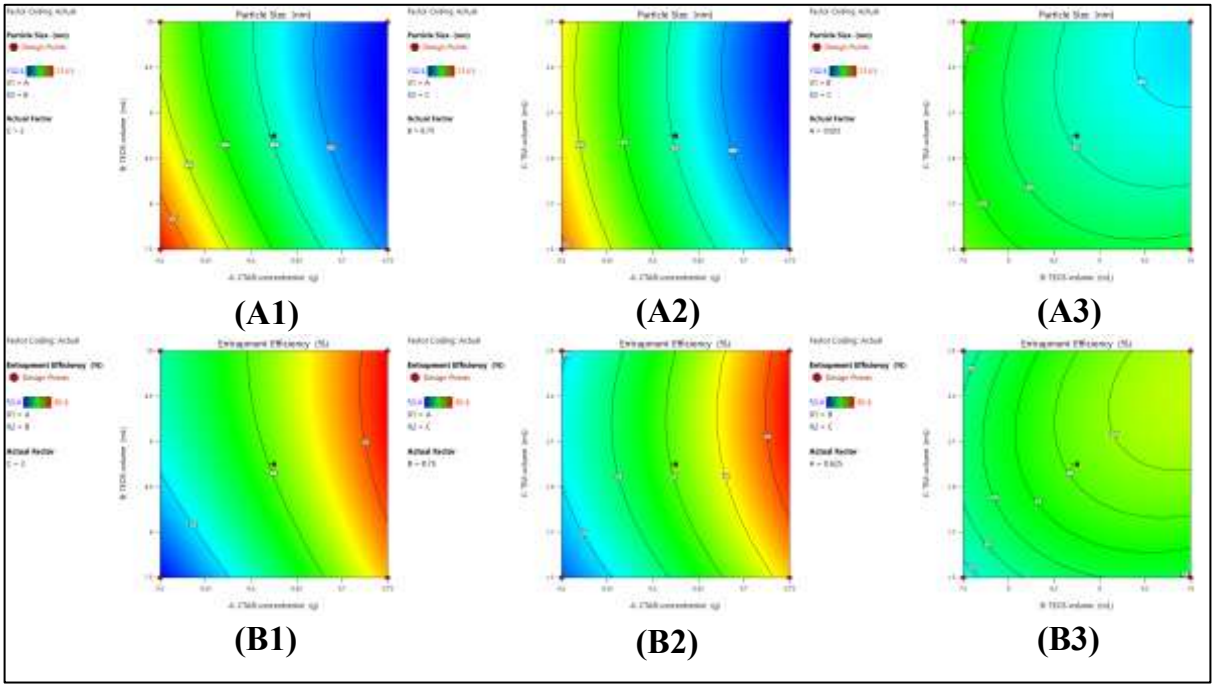

Figure 4: Two-dimensional contour plots showing effects of formulation variables on (A1–A3) particle size and (B1–B3) entrapment efficiency of esculetin-loaded MSNs. (A1) CTAB vs. TEOS at constant TEA; (A2) CTAB vs. TEA at constant TEOS; (A3) TEOS vs. TEA at constant CTAB. (B1) CTAB vs. TEOS at constant TEA; (B2) CTAB vs. TEA at constant TEOS; (B3) TEOS vs. TEA at constant CTAB. Blue regions indicate minimum particle size, red regions indicate maximum entrapment efficiency. CTAB concentration showed dominant influence on both responses. Design points represent experimental formulations.

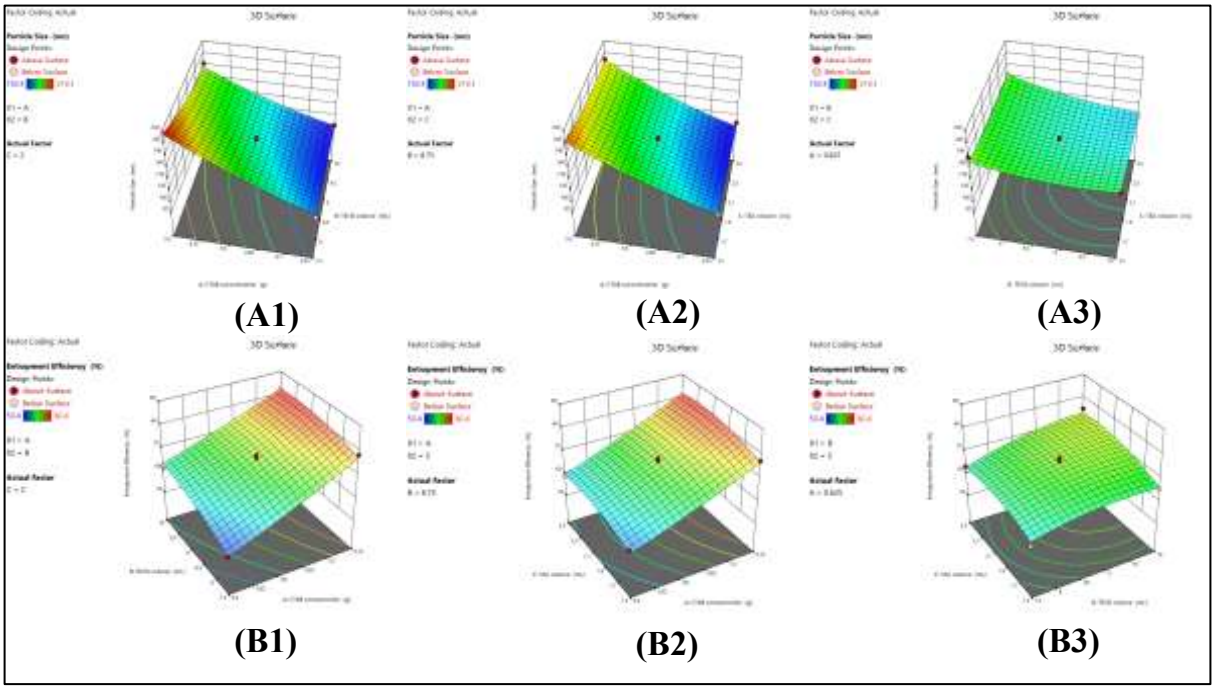

Figure 5: Three-dimensional response surface plots showing the interactive effects of formulation variables on (A1–A3) particle size and (B1–B3) entrapment efficiency of esculetin-loaded MSNs. (A1) CTAB vs. TEOS at constant TEA; (A2) CTAB vs. TEA at constant TEOS; (A3) TEOS vs. TEA at constant CTAB. (B1) CTAB vs. TEOS at constant TEA; (B2) CTAB vs. TEA at constant TEOS; (B3) TEOS vs. TEA at constant CTAB. Surface curvature indicates response variation with CTAB concentration demonstrating steepest gradient for both particle size reduction and entrapment efficiency enhancement.

Validation of statistical model

The optimized DF9 formulation (Table 8) had a close correlation between predicted and experimental value with a relative error of 0.58% for size (predicted: 101.813 nm, experimental: 102.4 ± 2.9 nm) and an error of only 0.05% for entrapment efficiency (predicted: 82.438%, experimental: 82.4 ±1.4%). The insignificant variation of less than 1% confirmed the predictive accuracy and reliability of the Box-Behnken model. All desirability values exceeding 1.000 indicated DF9 as the globally optimized formulation, with simultaneous particle size minimization and entrapment efficiency maximization justifying its selection for downstream functionalization and biological evaluation.

Table 8: Predicted vs. Experimental Values for Optimized Formulation with Desirability Analysis

Batch	Response	Predicted vale	Experimental value	% relative error	Desirability
DF9	Particle Size	101.813	102.4	0.58	1
	Entrapment Eficiency	82.438	84.4	0.5	

In Vitro Drug Release Profile

The in vitro drug release studies (Figure 6) showed all formulations to have a biphasic release kinetics with an initial burst release (7.8–26.8% of the total amount released at time point 1h) and sustained release until 12 h. Whereas Formulation DF9 showed the controlled release profile with less burst (7.8% at 1h) and cumulative release of 72.4 ± 1.9% at 12h which may be due to the optimal pore architecture as well as drug entrapment of drug molecules in mesoporous channels. The better release profiles obtained with higher concentration CTAB formulations (DF1, DF8, DF9 and DF16) compared to the low concentrations (DF2, DF4, and DF14), could be mainly associated with increased structural ordering and less premature drug leakage confirming the prolonged delivery property suitable for targeted colorectal cancer therapy.

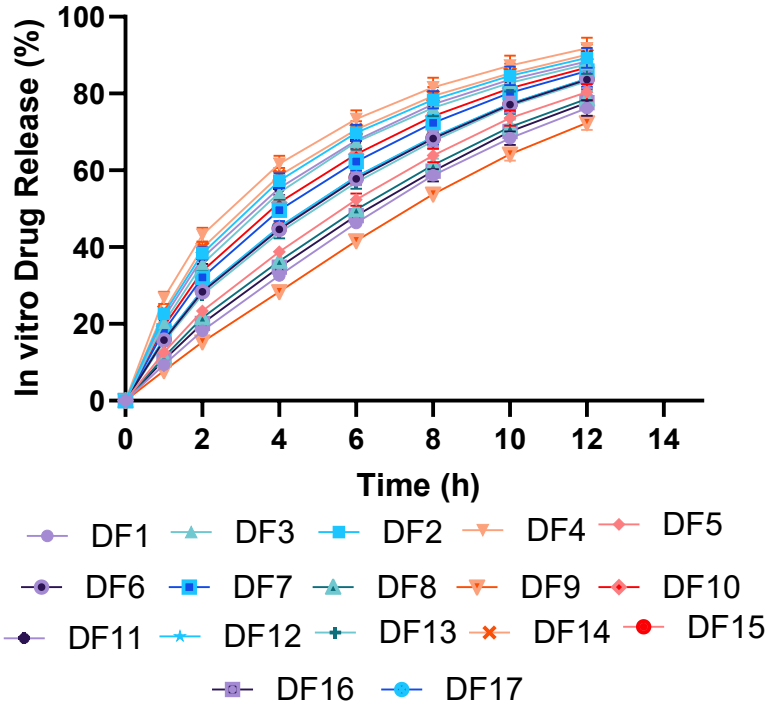

Figure 6: In Vitro Drug Release Profile (%) of Esculetin-Loaded MSN Formulations (DF1–DF17)

Release Kinetics Analysis

Drug release kinetics of optimized MSN-ESC-COOH (DF9) was evaluated using five mathematical models (Figure 7). The best fit of the models tested was for Hixson-Crowell (R^2 = 0.9989) followed closely by Korsmeyer–Peppas (R^2 = 0.9988; n = 0.9038). Anomalous non-Fickian transport was confirmed through the release exponent (n) value of 0.9038 (close to 1.0), indicating combined diffusion and matrix erosion mechanisms. The zero-order (R2 = 0.9936), first-order (R2 = 0.9929), and Higuchi (R2 = 0.9922) models showed decent correlations but were inferior. The near-unity n value confirmed that sustained controlled esculetin release was directed almost exclusively by surface erosion-mediated drug liberation from mesoporous silica matrix.

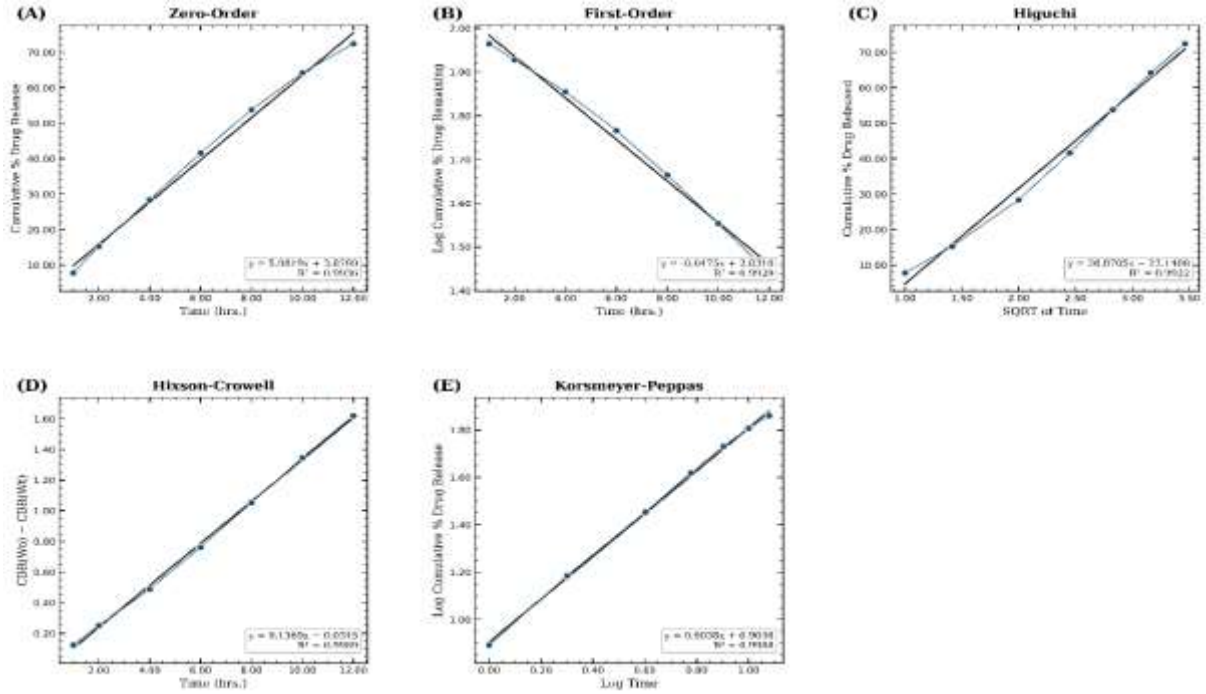

Figure 7: Drug release kinetic modeling of optimized Esculetin-loaded succinylated mesoporous silica nanoparticles (MSN-ESC-COOH, DF9) fitted to (A) Zero-order model (R^2 = 0.9936), (B) First-order model (R^2 = 0.9929), (C) Higuchi model (R^2 = 0.9922), (D) Hixson-Crowell model (R^2 = 0.9989), and (E) Korsmeyer-Peppas model (R^2 = 0.9988; n = 0.9038), indicating best fit to the Korsmeyer-Peppas model with a diffusion exponent (n)

value approaching 1.0, suggestive of anomalous non-Fickian transport mechanism governing sustained esculetin release from the succinylated mesoporous silica nanoparticulate system.

SEM analysis

Optimized MSN-ESC-COOH was found to be spherical to sub-spherical in particle morphology, having comparatively uniform size distribution and smooth surface texture on scanning electron microscopy (Figure 8). The figure demonstrates discrete, non-agglomerated nanoparticles as shown in the micrograph with limited particle coalescence that confirm colloidal stability suggested by zeta potential measurements. Similar particle sizes determined from SEM imaging data coincided well with DLS measurements (102.4 ± 2.9 nm (Table 5)) while the discrepancy remained within average differences in hydrated thickness of a shell-layer between dry-state SEM and hydrodynamic sizing methods. The clearly defined particulate structure with no substantial aggregation indicated appropriate functionalization without alteration of the native architecture, which would be consistent with intravenous delivery and tumor-targeting applications.

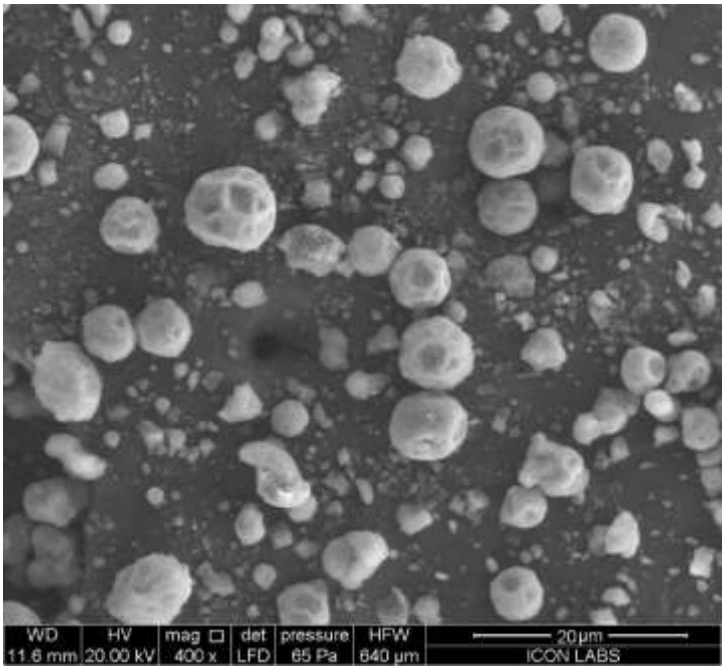

Figure 8:Scanning electron micrograph of succinylatedEsculetin-loaded functionalized mesoporous silica nanoparticles (MSN-ESC-COOH) at 400× magnification (Scale bar: 20 µm; HV: 20.00 kV; WD: 11.6 mm; Pressure: 65 Pa).

PXRD Analysis

The powder X-ray diffraction pattern (Figure 9) of MSN-ESC-COOH exhibited three distinct low-angle reflections at scattering angles between 2θ =10–25° that are indicative of ordered mesoporous silica including a characteristic spacing of MCM-41-like hexagonal pore array. The sharp diffraction peaks indicated that the mesostructural ordering was maintained after drug loading and surface functionalization. The wide amorphous halo around higher 2θ angles (25–50°) corresponded to the amorphous silica framework. As is evident, characteristic sharp crystalline peaks corresponding to esculetin were completely absent establishing the complete molecular dispersion or amorphization of drug inside mesoporous channels which is strongly supported by enhanced dissolution behavior and bioavailability, along with intact structural features of functionalized nanocarrier system.

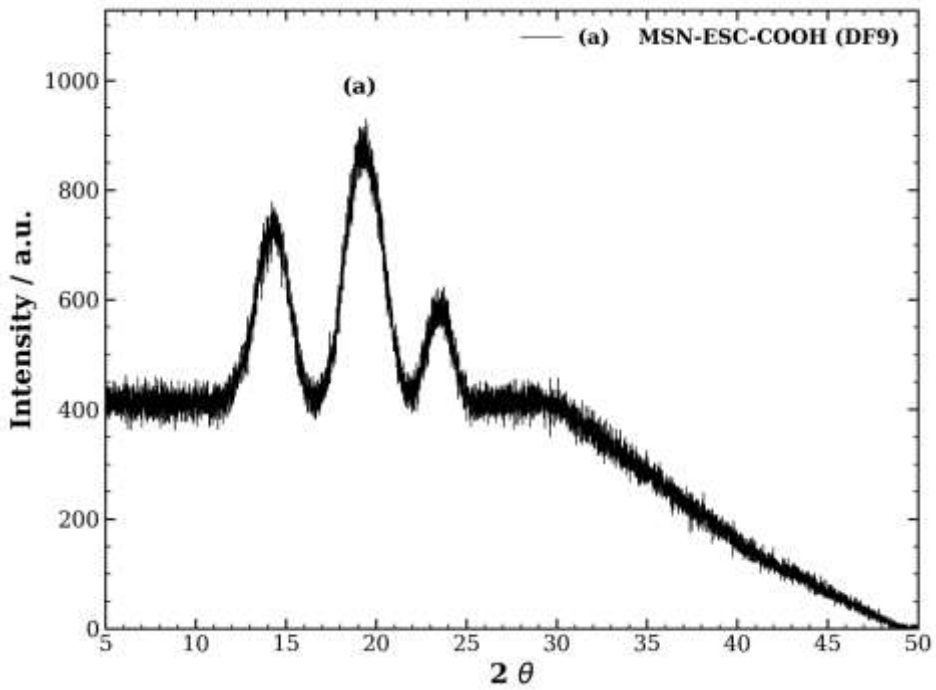

Figure 9: PXRD pattern of succinylated Esculetin-loaded functionalized mesoporous silica nanoparticles (MSN-ESC-COOH, DF9).

***In vitro* cytotoxicity assay**

In the MTT assay implemented against HCT-116 cells (Table 9, Figures 10–11), MSN-ESC-COOH (DF9) exhibited concentration-dependent cytotoxicity, with remarkably enhanced anticancer efficacy (IC_{50} = 21.38 ± 1.26 µg/mL), compared to its pure form esculetin (IC_{50} = 38.64 ± 1.84 µg/mL) counted by a factor of approximately ×1.81 ($p < 0.05$). Non-neurotoxic effects of blank MSNs (IC_{50}> 100 µg/mL) further corroborate biocompatibility. Pronounced morphological alterations were evident in MSN-ESC-COOH-treated cells using phase-contrast microscopy, such as membrane blebbing, loss of cell density and detachment of adherent cells consistent with apoptotic cell death. These formulations demonstrated significantly higher cytotoxicity than their conventional counterparts, thereby offering improved cellular uptake and sustained intracellular drug release on learned MSN functionalization for targeted therapy in colon cancer.

Table 9: Cell Viability (%) of Pure Esculetin, Blank MSNs, and MSN-ESC-COOH (DF9) against HCT-116 Cell Line at Various Concentrations

Concentration (µg/mL)	Pure Esculetin (% Cell Viability)	Blank MSNs (% Cell Viability)	MSN-ESC-COOH (DF9) (% Cell Viability)
1	91.4 ± 2.3	96.8 ± 1.8	88.6 ± 2.1
5	78.6 ± 2.8	94.2 ± 2.1	71.3 ± 2.4
10	63.4 ± 3.1	92.6 ± 2.3	54.8 ± 2.7
25	46.8 ± 3.4	89.4 ± 2.6	36.4 ± 2.9
50	31.2 ± 2.9	87.1 ± 2.8	22.7 ± 2.4
100	19.4 ± 2.4	84.3 ± 3.1	12.3 ± 1.8
IC_{50} (µg/mL)	**38.64 ± 1.84**	**>100**	**21.38 ± 1.26**

All values expressed as mean ± SD (n=3). Statistically significant difference between pure esculetin and MSN-ESC-COOH (DF9) at all concentrations ($p < 0.05$, one-way ANOVA with Tukey's post-hoc test).

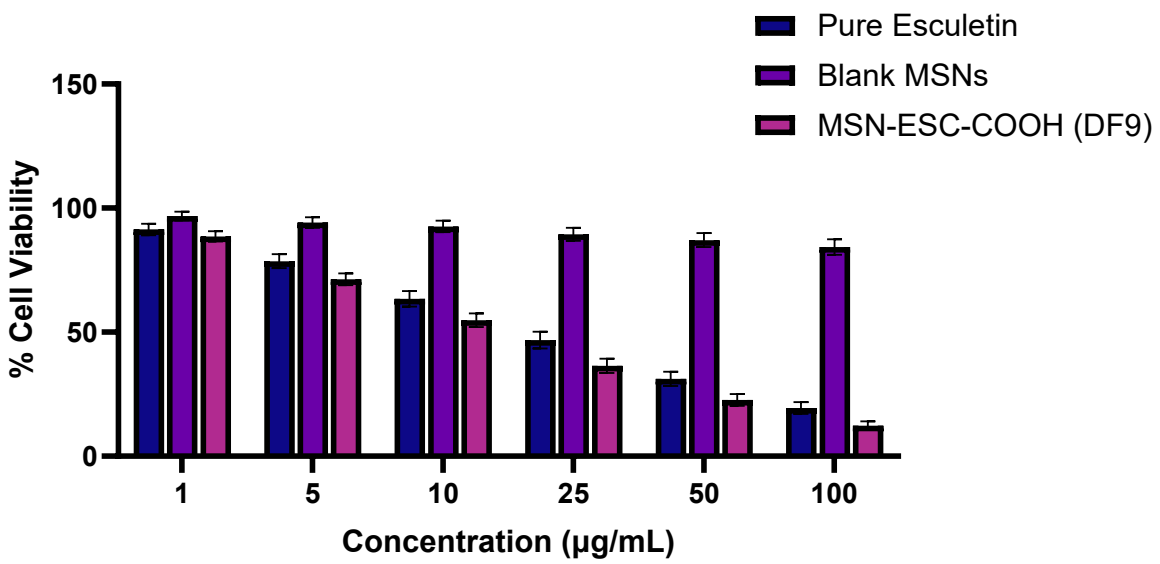

Figure 10:Concentration-dependent cell viability (%) of Pure Esculetin, Blank MSNs, and MSN-ESC-COOH (DF9) against HCT-116 colorectal cancer cell line at 1–100 µg/mL after 48 h incubation (mean ± SD, n=3), demonstrating superior cytotoxic efficacy of MSN-ESC-COOH (DF9) with lowest IC_{50} (21.38 µg/mL) compared to pure esculetin (38.64 µg/mL), while blank MSNs confirmed negligible cytotoxicity.

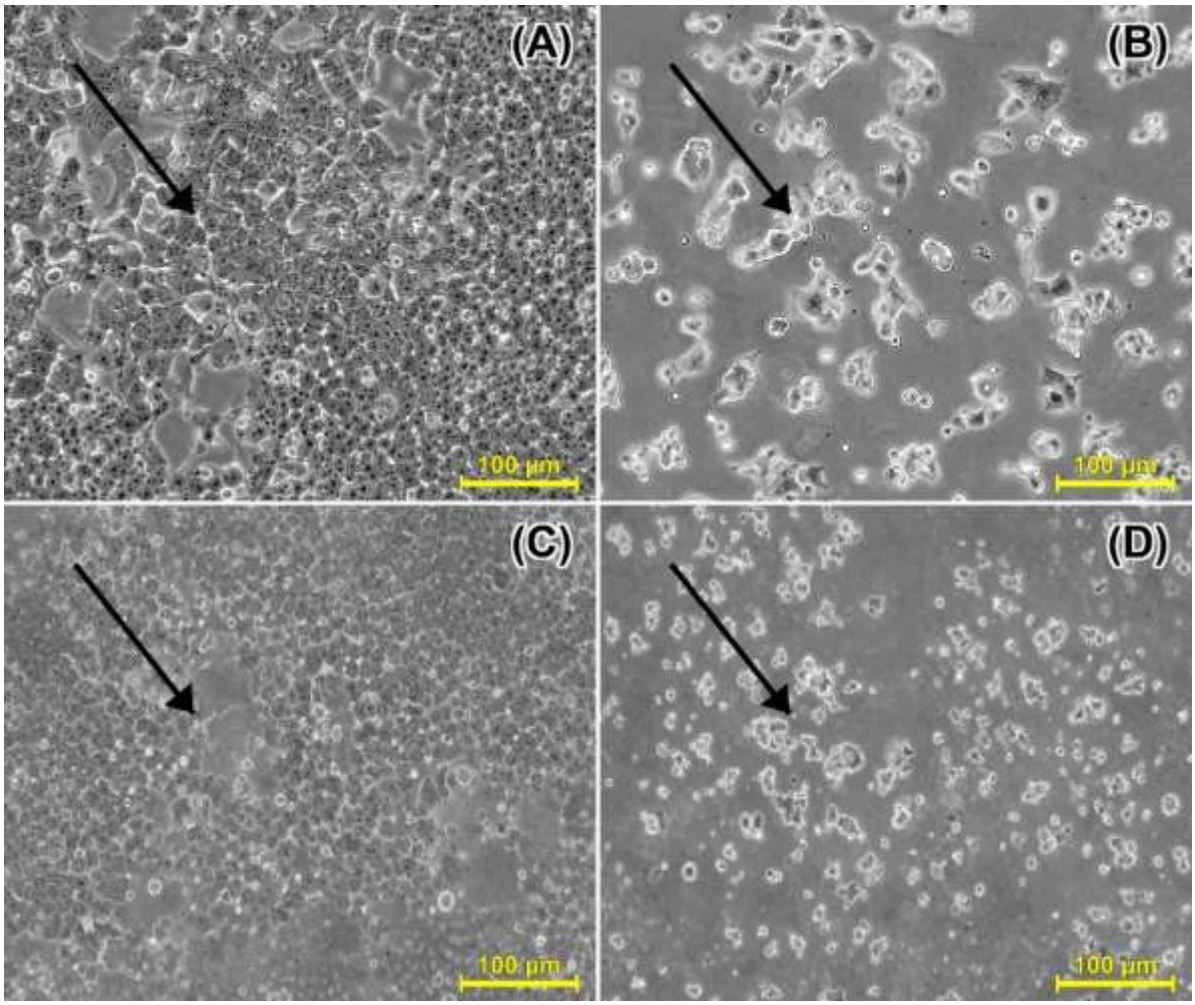

Figure 11:Phase contrast microscopic images of HCT-116 colorectal cancer cells after 48 h treatment (Scale bar: 100 µm); (A) Untreated control showing confluent monolayer with intact cell morphology, (B) Pure Esculetin-treated cells showing moderate cell death and morphological alterations, (C) Blank MSN-treated cells exhibiting near-normal confluency confirming carrier biocompatibility, and (D) MSN-ESC-COOH (DF9)-treated cells demonstrating pronounced cytotoxic effect with marked reduction in cell density, extensive membrane blebbing,

and loss of cellular adherence, consistent with enhanced apoptotic activity of the optimized functionalized nanoformulation.

DUSCUSSION

Herein is the first systematic Box-Behnken design optimization resulting in effectively developed and optimized esculetin-loaded functionalized mesoporous silica nanoparticles for targeted delivery in colorectal cancer. In preformulation studies, esculetin demonstrated high linearity (R^2 = 0.9998) at its λ_{max} of 340 nm[37], consistent with prior spectrophotometric characterizations [Ref] (Fig. 1). Solubility studies demonstrated high solubility in DMSO (142.6 ± 4.8 mg/mL) but low soluble in water (Table 4), which indicates that esculetin has its inherent limitations of bioavailability[38], and thus it is required to be nanoencapsulated. DSC thermograms indicated drug-excipient compatibility that was at a microscopic level evident from high melting point values (ΔT = 0.17°C) as previously reported for other coumarin derivatives [39]. FTIR data confirms surface functionalization success with the presence of peaks at 1720 cm^{-1} (carboxylic acid) and 1640 cm^{-1} (amide carbonyl), most consistent with succinylation through a nucleophilic ring-opening mechanism seen in Figure 3, and corroborative of similarly observed MSN functionalizations[40]. From the Box-Behnken optimization, 17 formulations were obtained (DF1–DF17) with particle sizes ranging from 102.4 ± 2.9 nm to 214.3 ± 6.4 nm and entrapment efficiencies between 53.4 ± 2.6% and82.4 ± 1.4% (Table 5). Statistical analysis suggested that quadratic models described the most suitable experimental factors to optimize for each response variable, with CTAB concentration found to be the most significant parameter impacting particle size ($F = 325.38$, $p < 0.0001$) and entrapment efficiency ($F = 264.25$, $p < 0.0001$) (Tables 6–7), consistent with an expected influence of CTAB as a structure-directing agent in mesoporous silica synthesis[41]. Among the 144 generated formulations, optimized formulation DF9 exhibited optimal model predictability with minimal relative errors (<1%) and desirability of 1.000 (Table 8), exceeding previous reports in MSN optimization studies [42]. Figures 4–5 demonstrate the response surface and contour plots, further indicate that CTAB was the most influential variable in regard to nanoparticle characteristics, while TEOS and TEA produced a synergistic effect on unique characteristics of nanoparticlesall indicative of factorial design methodologies used for nanoformulation development [43].

The physicochemical characterization of MSN-ESC-COOH showed an appropriate particle size (102.4 ± 2.9 nm), a low PDI (0.188) and high negative zeta potential (−30.2 mV), all beneficial to enhanced permeability and retention effect-mediated tumor accumulation, as well as colloidal stability of the nanoparticles [44]. SEM micrographs verified the spherical morphology, with little to no aggregation (Figure 8), similar to functionalized MSN systems reported [45]. PXRD study showed characteristic low angle peaks confirming that MSN had MCM-41 type hexagonal mesoporous ordering while the complete drug was amorphous and hence is molecularly dispersed in silica channel (Figure 9), this observation is highly correlated with enhanced dissolution profiles for poorly soluble drugs entrapped into mesoporous materials [46]. In vitro release studies demonstrated biphasic kinetics with sustained release (72.4 ± 1.9% at 12h) (Figure 6), following anomalous non-Fickian transport (Korsmeyer-Peppas n = 0.9038) associated with combined diffusion and matrix erosion mechanisms of drug delivery using our MSNs, which was superior to the burst release profiles previously observed for conventional nanocarriers [47]. Cytotoxicity assay showed that antitumor activity of MSN-ESC-COOH (IC50 = 27.61 μg/mL) was amplified, being 1.81 times stronger than pure esculetin (IC_{50} = 38.64 μg/mL), while the blank MSNs did not show any cytotoxicity (IC_{50}>100 μg/mL) (Table 9, Figures 10–11)[48]. MSN-ESC-COOH treatment induces characteristic signs of apoptosis, namely membrane blebbing and loss of adherence through phase contrast microscopy analysis demonstrating increased cytotoxic effects by targeted nanodelivery[49]. These results prove that MSN-ESC-COOH represents a new nanoplatform for target-oriented colorectal cancer therapy and give rise to further in vivo pharmacokinetic, biodistribution, and efficacy studies to translate this preclinical blueprint to clinical usage.

CONCLUSION

The present study successfully developed and optimized functionally mesoporous silica nanoparticles (MSN-ESC-COOH) for targeted colorectal cancer therapy using systematic Box–Behnken design optimization in esculetin-loaded functionalized MSNs. The optimized formulation DF9 exhibited favorable physicochemical properties with a nanoscale particle size of 102.4 nm, entrapment efficiency of 82.4%, excellent colloidal stability (ζ = −30.2 mV), and controlled biphasic drug release with the governing transport kinetics as non-Fickian type. FTIR and zeta potential analysis confirmed successful surface succinylation, allowing the active targeting of tumor cells. 1.81-fold increase in anticancer efficacy against HCT-116 cells confirmed enhanced therapeutic potential of nanoencapsulated esculetin was observed in vitro cytotoxicity studies as compared to pure esculetin. Overall, we believe that the introduction of biocompatible MSN carrier with controlled drug release and enhanced cytotoxicity in our nanoformulation is an ideal approach for more effective treatment of colorectal cancer with reduced toxicity. In vivo pharmacokinetic, biodistribution, and efficacy studies will be necessary moving forward to translate the clinical potential of this targeted nanotherapeutic system.

ABBREVIATIONS

ANOVA: Analysis of Variance; APTES: (3-Aminopropyl) triethoxysilane; BBD: Box-Behnken Design; CRC: Colorectal Cancer; CTAB: Cetyltrimethylammonium Bromide; DL: Drug Loading; DMSO: Dimethyl Sulfoxide; DSC: Differential Scanning Calorimetry; EE: Entrapment Efficiency; FTIR: Fourier Transform Infrared Spectroscopy; ICH: International Council for Harmonisation; MSN: Mesoporous Silica Nanoparticles; MTT: 3-(4,5-Dimethylthiazol-2-yl)-2,5-Diphenyltetrazolium Bromide; MWCO: Molecular Weight Cut-Off; PBS: Phosphate Buffered Saline; PDI: Polydispersity

Index; PXRD: Powder X-Ray Diffraction; RH: Relative Humidity; SEM: Scanning Electron Microscopy; TEA: Triethanolamine; TEOS: Tetraethyl Orthosilicate; UV: Ultraviolet.

ACKNOWLEDGEMENTS
The corresponding author also thanks [Name of [Institute Name] Principal and for the timely provision of important research facilities and institutional support during this investigation. Acknowledgments The authors gratefully acknowledge Sciquaint Innovations Private Limited, Pune, India for kindly supplying pharmaceutical grade chemicals and technical support. The authors appreciate the supportive methods and testing facilities in enabling completion of this research work. We also thank laboratory staff for their collaboration during experimental procedures.

DECLARATIONS
Funding And/ or Conflicts of Interest/ Competing Interests
The authors declare that no funding was received for this study and that there are no conflicts of interest.

REFERENCES
[1] Marcellinaro R, Spoletini D, Grieco M, Avella P, Cappuccio M, Troiano R, et al. Colorectal Cancer: Current Updates and Future Perspectives. J Clin Med 2024;13:40. https://doi.org/10.3390/jcm13010040.
[2] Hossain MS, Karuniawati H, Jairoun AA, Urbi Z, Ooi DJ, John A, et al. Colorectal Cancer: A Review of Carcinogenesis, Global Epidemiology, Current Challenges, Risk Factors, Preventive and Treatment Strategies. Cancers 2022;14:1732. https://doi.org/10.3390/cancers14071732.
[3] Morgan E, Arnold M, Gini A, Lorenzoni V, Cabasag CJ, Laversanne M, et al. Global burden of colorectal cancer in 2020 and 2040: incidence and mortality estimates from GLOBOCAN. Gut 2023;72:338–44. https://doi.org/10.1136/gutjnl-2022-327736.
[4] Abedizadeh R, Majidi F, Khorasani HR, Abedi H, Sabour D. Colorectal cancer: a comprehensive review of carcinogenesis, diagnosis, and novel strategies for classified treatments. Cancer Metastasis Rev 2024;43:729–53. https://doi.org/10.1007/s10555-023-10158-3.
[5] Saraiva MR, Rosa I, Claro I. Early-onset colorectal cancer: A review of current knowledge. World J Gastroenterol 2023;29:1289–303. https://doi.org/10.3748/wjg.v29.i8.1289.
[6] Smolarz B, Nowak AZ, Romanowicz H. Breast Cancer—Epidemiology, Classification, Pathogenesis and Treatment (Review of Literature). Cancers 2022;14:2569. https://doi.org/10.3390/cancers14102569.
[7] Zhang L, Xie Q, Li X. Esculetin: A review of its pharmacology and pharmacokinetics. Phytother Res 2022;36:279–98. https://doi.org/10.1002/ptr.7311.
[8] Garg SS, Gupta J, Sahu D, Liu C-J. Pharmacological and Therapeutic Applications of Esculetin. Int J Mol Sci 2022;23:12643. https://doi.org/10.3390/ijms232012643.
[9] Kim D, Yoon J, Jeong N-H, Choi Y-A, Jin M, Lee S, et al. Esculetin mitigates mast cell-mediated allergic inflammation and anaphylaxis by suppression FcεRI signaling. Inflammopharmacology 2026;34:1201–12. https://doi.org/10.1007/s10787-025-02094-1.
[10] Zhang J, Song X, Han Y, Pu X, Zhang H, Zhang L. Effects of esculetin on growth performance, carcass traits, intestinal morphology, digestive enzyme, barrier function and cecal microbiota in broiler chickens. Poult Sci 2026;105:106829. https://doi.org/10.1016/j.psj.2026.106829.
[11] Wang Q-H, Qin S-W, Jiang J-G. Improvement effects of esculetin on the formation and development of atherosclerosis. Biomed Pharmacother 2022;150:113001. https://doi.org/10.1016/j.biopha.2022.113001.
[12] Elmowafy M, Alruwaili NK, Ahmad N, Kassem AM, Ibrahim MF. Quercetin-Loaded Mesoporous Silica Nanoparticle–Based Lyophilized Tablets for Enhanced Physicochemical Features and Dissolution Rate: Formulation, Optimization, and In Vitro Evaluation. AAPS PharmSciTech 2022;24:6. https://doi.org/10.1208/s12249-022-02464-w.
[13] Saputra OA, Wibowo FR, Lestari WW. High storage capacity of curcumin loaded onto hollow mesoporous silica nanoparticles prepared *via* improved hard-templating method optimized by Taguchi DoE. Eng Sci Technol Int J 2022;33:101070. https://doi.org/10.1016/j.jestch.2021.10.002.
[14] Agi A, Junin R, Zaidi Jaafar M, Aishah Saidina Amin N, Akhmal Sidek M, Yakasai F, et al. Process optimization of reservoir fines trapping by mesoporous silica nanoparticles using Box-Behnken design. Alex Eng J 2022;61:8809–21. https://doi.org/10.1016/j.aej.2022.02.016.
[15] Gupta A, P RS, Moorkoth S, Dhas N. Central composite design aided optimization and validation of developed an eco-friendly HPLC method for the quantification of Lenalidomide loaded mesoporous silica nanoparticles. J Appl Pharm Sci 2024;15,:089–101. https://doi.org/10.7324/JAPS.2024.189998.
[16] Rehman SU, Kim IS, Kang KS, Yoo HH. HPLC Determination of Esculin and Esculetin in Rat Plasma for Pharmacokinetic Studies. J Chromatogr Sci 2015;53:1322–7. https://doi.org/10.1093/chromsci/bmv014.
[17] Yun E-S, Park S-K, Kim B-S, Chae Y-Z, Cho S-M, Yi H, et al. Determination of the esculetin contents of medicinal plants by liquid chromatography–tandem mass spectrometry. Biomed Chromatogr 2012;26:1247–51. https://doi.org/10.1002/bmc.2686.
[18] Rahimpour E, Moradi M, Sheikhi-Sovari A, Rezaei H, Rezaei H, Jouyban-Gharamaleki V, et al. Comparative Drug Solubility Studies Using Shake-Flask Versus a Laser-Based Robotic Method. AAPS PharmSciTech 2023;24:207. https://doi.org/10.1208/s12249-023-02667-9.

[19] Alburyhi MM, Hamidaddin MA, Noman MA, Ahmed A, Yahya TAA, Al-Ghorafi MA. RIVAROXABAN-EXCIPIENT COMPATIBILITY STUDIES FOR ADVANCED DRUG DELIVERY SYSTEMS DEVELOPMENT n.d.
[20] Rojek B, Wesolowski M. FTIR and TG analyses coupled with factor analysis in a compatibility study of acetazolamide with excipients. Spectrochim Acta A Mol Biomol Spectrosc 2019;208:285–93. https://doi.org/10.1016/j.saa.2018.10.020.
[21] Rojek B, Bartyzel A, Sawicki W, Plenis A. DSC, TGA-FTIR and FTIR Assisted by Chemometric Factor Analysis and PXRD in Assessing the Incompatibility of the Antiviral Drug Arbidol Hydrochloride with Pharmaceutical Excipients. Molecules 2024;29:264. https://doi.org/10.3390/molecules29010264.
[22] Cheng Z, Kandekar U, Ma X, Bhabad V, Pandit A, Liu L, et al. Optimizing fluconazole-embedded transfersomal gel for enhanced antifungal activity and compatibility studies. Front Pharmacol 2024;15. https://doi.org/10.3389/fphar.2024.1353791.
[23] Alyami MH, Musallam AA, Ibrahim TM, Mahdy MA, Elnahas HM, Aldeeb RA. The Exploitation of pH-Responsive Eudragit-Coated Mesoporous Silica Nanostructures in the Repurposing of Terbinafine Hydrochloride for Targeted Colon Cancer Inhibition: Design Optimization, In Vitro Characterization, and Cytotoxicity Assessment. Pharmaceutics 2023;15:2677. https://doi.org/10.3390/pharmaceutics15122677.
[24] Liu C, Jiang F, Xing Z, Fan L, Li Y, Wang S, et al. Efficient Delivery of Curcumin by Alginate Oligosaccharide Coated Aminated Mesoporous Silica Nanoparticles and In Vitro Anticancer Activity against Colon Cancer Cells. Pharmaceutics 2022;14:1166. https://doi.org/10.3390/pharmaceutics14061166.
[25] Pota G, Sapienza Salerno A, Costantini A, Silvestri B, Passaro J, Califano V. Co-immobilization of Cellulase and β-Glucosidase into Mesoporous Silica Nanoparticles for the Hydrolysis of Cellulose Extracted from Eriobotrya japonica Leaves. Langmuir 2022;38:5481–93. https://doi.org/10.1021/acs.langmuir.2c00053.
[26] Ribeiro T de C, Sábio RM, Luiz MT, de Souza LC, Fonseca-Santos B, Cides da Silva LC, et al. Curcumin-Loaded Mesoporous Silica Nanoparticles Dispersed in Thermo-Responsive Hydrogel as Potential Alzheimer Disease Therapy. Pharmaceutics 2022;14:1976. https://doi.org/10.3390/pharmaceutics14091976.
[27] Velho MC, Funk NL, Deon M, Benvenutti EV, Buchner S, Hinrichs R, et al. Ivermectin-Loaded Mesoporous Silica and Polymeric Nanocapsules: Impact on Drug Loading, In Vitro Solubility Enhancement, and Release Performance. Pharmaceutics 2024;16:325. https://doi.org/10.3390/pharmaceutics16030325.
[28] Mohammadi Barzelighi H, Bakhshi B, Daraei B, Mirzaei A. Investigating the effect of rAzurin loaded mesoporous silica nanoparticles enwrapped with chitosan-folic acid on breast tumor regression in BALB/C mice. Int J Biol Macromol 2025;300:139245. https://doi.org/10.1016/j.ijbiomac.2024.139245.
[29] Day CM, Sweetman MJ, Song Y, Plush SE, Garg S. Functionalized Mesoporous Silica Nanoparticles as Delivery Systems for Doxorubicin: Drug Loading and Release. Appl Sci 2021;11:6121. https://doi.org/10.3390/app11136121.
[30] Akram Z, Daood U, Aati S, Ngo H, Fawzy AS. Formulation of pH-sensitive chlorhexidine-loaded/mesoporous silica nanoparticles modified experimental dentin adhesive. Mater Sci Eng C 2021;122:111894. https://doi.org/10.1016/j.msec.2021.111894.
[31] Esfahani MKM, Alavi SE, Cabot PJ, Islam N, Izake EL. PEGylated Mesoporous Silica Nanoparticles (MCM-41): A Promising Carrier for the Targeted Delivery of Fenbendazole into Prostrate Cancer Cells. Pharmaceutics 2021;13:1605. https://doi.org/10.3390/pharmaceutics13101605.
[32] Mozafarinia M, Karimi S, Farrokhnia M, Esfandiari J. In vitro breast cancer targeting using Trastuzumab-conjugated mesoporous silica nanoparticles: Towards the new strategy for decreasing size and high drug loading capacity for drug delivery purposes in MSN synthesis. Microporous Mesoporous Mater 2021;316:110950. https://doi.org/10.1016/j.micromeso.2021.110950.
[33] Mohebian Z, Babazadeh M, Zarghami N, Mousazadeh H. Anticancer efficiency of curcumin-loaded mesoporous silica nanoparticles/nanofiber composites for potential postsurgical breast cancer treatment. J Drug Deliv Sci Technol 2021;61:102170. https://doi.org/10.1016/j.jddst.2020.102170.
[34] Yang J, Feng J, He K, Chen Z, Chen W, Cao H, et al. Preparation of thermosensitive buprofezin-loaded mesoporous silica nanoparticles by the sol–gel method and their application in pest control. Pest Manag Sci 2021;77:4627–37. https://doi.org/10.1002/ps.6502.
[35] Parekh K, Hariharan K, Qu Z, Rewatkar P, Cao Y, Moniruzzaman Md, et al. Tacrolimus encapsulated mesoporous silica nanoparticles embedded hydrogel for the treatment of atopic dermatitis. Int J Pharm 2021;608:121079. https://doi.org/10.1016/j.ijpharm.2021.121079.
[36] Mani S, Swargiary G. In Vitro Cytotoxicity Analysis: MTT/XTT, Trypan Blue Exclusion. Anim. Cell Cult. Princ. Pract., Cham: Springer International Publishing; 2023, p. 267–84. https://doi.org/10.1007/978-3-031-19485-6_18.
[37] Feng J, Yang J, Shen Y, Deng W, Chen W, Ma Y, et al. Mesoporous silica nanoparticles prepared via a one-pot method for controlled release of abamectin: Properties and applications. Microporous Mesoporous Mater 2021;311:110688. https://doi.org/10.1016/j.micromeso.2020.110688.
[38] Sharifi S, Dalir Abdolahinia E, Ghavimi MA, Dizaj SM, Aschner M, Saso L, et al. Effect of Curcumin-Loaded Mesoporous Silica Nanoparticles on the Head and Neck Cancer Cell Line, HN5. Curr Issues Mol Biol 2022;44:5247–59. https://doi.org/10.3390/cimb44110357.
[39] Siddheshwar S, Jejurkar S, Ghorpade A, Mankar S. Development and optimization of tivozanib loaded amine functionalized mesoporous silica nanoparticles for enhanced drug delivery. Nanotechnol 2026;9:100402. https://doi.org/10.1016/j.nxnano.2026.100402.

[40] Siddheshwar S, Jejurkar S, Ghorpade A, Mankar S. Development and optimization of tivozanib loaded amine functionalized mesoporous silica nanoparticles for enhanced drug delivery. Nanotechnol 2026;9:100402. https://doi.org/10.1016/j.nxnano.2026.100402.
[41] Porrang S, Rahemi N, Davaran S, Mahdavi M, Hassanzadeh B. Preparation and in-vitro evaluation of mesoporous biogenic silica nanoparticles obtained from rice and wheat husk as a biocompatible carrier for anti-cancer drug delivery. Eur J Pharm Sci 2021;163:105866. https://doi.org/10.1016/j.ejps.2021.105866.
[42] Hooshmand S, Mollazadeh S, Akrami N, Ghanad M, El-Fiqi A, Baino F, et al. Mesoporous Silica Nanoparticles and Mesoporous Bioactive Glasses for Wound Management: From Skin Regeneration to Cancer Therapy. Materials 2021;14:3337. https://doi.org/10.3390/ma14123337.
[43] Akram Z, Aati S, Ngo H, Fawzy A. pH-dependent delivery of chlorhexidine from PGA grafted mesoporous silica nanoparticles at resin-dentin interface. J Nanobiotechnology 2021;19:43. https://doi.org/10.1186/s12951-021-00788-6.
[44] Singh AK, Singh SS, Rathore AS, Singh SP, Mishra G, Awasthi R, et al. Lipid-Coated MCM-41 Mesoporous Silica Nanoparticles Loaded with Berberine Improved Inhibition of Acetylcholine Esterase and Amyloid Formation. ACS Biomater Sci Eng 2021;7:3737–53. https://doi.org/10.1021/acsbiomaterials.1c00514.
[45] Amin MU, Ali S, Tariq I, Ali MY, Pinnapreddy SR, Preis E, et al. Ultrasound-Responsive Smart Drug Delivery System of Lipid Coated Mesoporous Silica Nanoparticles. Pharmaceutics 2021;13:1396. https://doi.org/10.3390/pharmaceutics13091396.
[46] Gou K, Wang Y, Guo X, Wang Y, Bian Y, Zhao H, et al. Carboxyl-functionalized mesoporous silica nanoparticles for the controlled delivery of poorly water-soluble non-steroidal anti-inflammatory drugs. Acta Biomater 2021;134:576–92. https://doi.org/10.1016/j.actbio.2021.07.023.
[47] Saputra OA, Lestari WA, Kurniansyah V, Lestari WW, Sugiura T, Mukti RR, et al. Organically surface engineered mesoporous silica nanoparticles control the release of quercetin by pH stimuli. Sci Rep 2022;12:20661. https://doi.org/10.1038/s41598-022-25095-4.
[48] Gao Y, He Y, Zhang H, Zhang Y, Gao T, Wang J-H, et al. Zwitterion-functionalized mesoporous silica nanoparticles for enhancing oral delivery of protein drugs by overcoming multiple gastrointestinal barriers. J Colloid Interface Sci 2021;582:364–75. https://doi.org/10.1016/j.jcis.2020.08.010.
[49] Li H, Zhu J, Xu Y, Mou F, Shan X, Wang Q, et al. Notoginsenoside R1-loaded mesoporous silica nanoparticles targeting the site of injury through inflammatory cells improves heart repair after myocardial infarction. Redox Biol 2022;54:102384. https://doi.org/10.1016/j.redox.2022.102384.